Bound Substrate in the Structure of Cyanobacterial Branching Enzyme Supports a New Mechanistic Model

Mari Hayashi, Ryuichiro Suzuki, Christophe Colleoni, Steven Ball, Naoko Fujita, Eiji Suzuki

THE JOURNAL OF BIOLOGICAL CHEMISTRY VOL. 292, NO. 13, pp. 5465–5475, March 31, 2017

Bound Substrate in the Structure of Cyanobacterial Branching Enzyme Supports a New Mechanistic Model*

Received for publication, September 2, 2016, and in revised form, January 25, 2017 Published, JBC Papers in Press, February 13, 2017, DOI 10.1074/jbc.M116.755629

Mari Hayashi (林真里)[‡1], Ryuichiro Suzuki (鈴木龍一郎)[‡1,2], Christophe Colleoni[§], Steven G. Ball[§], Naoko Fujita (藤田直子)[‡], and Eiji Suzuki (鈴木英治)[‡3]

From the [‡]Department of Biological Production, Faculty of Bioresource Sciences, Akita Prefectural University, Shimoshinjyo-Nakano, Akita 010-0195, Japan and the [§]Unité de Glycobiologie Structurale et Fonctionnelle, Unité Mixte de Recherche 8576, CNRS-Université des Sciences et Technologies de Lille, 59655 Villeneuve d'Ascq Cedex, France

Edited by Norma Allewell

Branching enzyme (BE) catalyzes the formation of α-1,6-glucosidic linkages in amylopectin and glycogen. The reaction products are variable, depending on the organism sources, and the mechanistic basis for these different outcomes is unclear. Although most cyanobacteria have only one BE isoform belonging to glycoside hydrolase family 13, *Cyanothece* sp. ATCC 51142 has three isoforms (BE1, BE2, and BE3) with distinct enzymatic properties, suggesting that investigations of these enzymes might provide unique insights into this system. Here, we report the crystal structure of ligand-free wild-type BE1 (residues 5–759 of 1–773) at 1.85 Å resolution. The enzyme consists of four domains, including domain N, carbohydrate-binding module family 48 (CBM48), domain A containing the catalytic site, and domain C. The central domain A displays a $(\beta/\alpha)_8$-barrel fold, whereas the other domains adopt β-sandwich folds. Domain N was found in a new location at the back of the protein, forming hydrogen bonds and hydrophobic interactions with CBM48 and domain A. Site-directed mutational analysis identified a mutant (W610N) that bound maltoheptaose with sufficient affinity to enable structure determination at 2.30 Å resolution. In this structure, maltoheptaose was bound in the active site cleft, allowing us to assign subsites −7 to −1. Moreover, seven oligosaccharide-binding sites were identified on the protein surface, and we postulated that two of these in domain A served as the entrance and exit of the donor/acceptor glucan chains, respectively. Based on these structures, we propose a substrate binding model explaining the mechanism of glycosylation/deglycosylation reactions catalyzed by BE.

Branching enzyme (BE[4]; EC.2.4.1.18) catalyzes the transglucosylation reaction of the α-glucan molecules glycogen and amylopectin by cleaving an α-1,4-linkage to form a new branch point via an α-1,6-linkage (1, 2). Glycogen and starch (primarily composed of amylopectin) are major carbohydrates that are accumulated for energy reserve in animals, plants, and microorganisms (3–6). Glycogen has a randomly branched structure and displays high water solubility. By contrast, amylopectin is a water-insoluble polymer due to an ordered pattern of branching structure called tandem cluster structure (7, 8). The discrete pattern of branching makes the amylopectin molecule display a much higher molecular weight than glycogen and exhibit distinct properties, such as crystallinity and gelatinization upon hydrothermal treatment (8, 9). The action of BEs significantly influences the structure and property of these polysaccharides.

Distinct types of BE have been identified in various organisms. BEs found in many bacteria display sequence similarities to those in animals, fungi, and plants (10). These BEs are also distantly similar to α-amylase and other amylolytic enzymes, and they are collectively classified into the glycoside hydrolase 13 (GH13) family in the CAZy database (a sequence-based database of carbohydrate-active enzymes) (11). As the number of GH13 family members became enormous, the family was subdivided into more than 40 subfamilies (12). The eukaryotic and bacterial BEs are classified into the GH13_8 and GH13_9 subfamilies, respectively (2, 12). In addition, a different type of BE belonging to GH57 has been identified exclusively in prokaryotes (2, 13).

Cyanothece sp. ATCC 51142 is a unicellular cyanobacterium that performs oxygenic photosynthesis as well as nitrogen fixation (14). Whereas most cyanobacteria produce glycogen, some species, including ATCC 51142 and *Cyanobacterium* NBRC 102756, produce amylopectin-like polysaccharide, designated as cyanobacterial starch (10, 15, 16). A strong correlation has been observed between the type of α-glucan produced and the number of BE genes. Glycogen-producing cyanobacteria have one BE each from the GH13_9 and GH57 (sub)families. By contrast, ATCC 51142 and NBRC 102756 contain two extra

* This work was supported in part by Shimadzu Science Foundation Grant 120003 (to R. S.) and JSPS KAKENHI Grants 15K18685 (to R. S.) and 16K07467 (to E. S.). The authors declare that they have no conflicts of interest with the contents of this article.

The atomic coordinates and structure factors (codes 5GQU, 5GQV, 5GQW, and 5GQX) have been deposited in the Protein Data Bank (http://wwpdb.org/).

[1] Both authors contributed equally to this work.
[2] To whom correspondence may be addressed. Tel.: 81-18-872-1652; Fax: 81-18-872-1681; E-mail: ryuichi@akita-pu.ac.jp.
[3] To whom correspondence may be addressed. Tel.: 81-18-872-1653; Fax: 81-18-872-1681; E-mail: esuzuki@akita-pu.ac.jp.

[4] The abbreviations used are: BE, branching enzyme; CBM, carbohydrate-binding module; cceBE1, BE1 from *Cyanothece* sp. ATCC 51142; CrISA1, isoamylase 1 from *C. reinhardtii*; DP, degree of polymerization; EcBE, BE from *E. coli*; G3, maltotriose; G5, maltopentaose; G6, maltohexaose; G7, maltoheptaose; G8, maltooctaose; G9, maltononaose; G10, maltodecaose; GH, glycoside hydrolase; HsBE, BE from *H. sapiens*; LF, ligand-free; MtBE, BE from *M. tuberculosis* H37RV; OsBEI, BEI from *O. sativa*; RMSD, root mean square deviation; SBS, surface binding site; WtBE1, WT of cceBE1; PDB, Protein Data Bank.

TABLE 1

Summary of data collection and refinement statistics for proteins investigated in this study

Values for the highest resolution shell are given in parentheses.

Parameters	Values			
	PDB code 5GQU	PDB code 5GQV	PDB code 5GQW	PDB code 5GQX
Data collection statistics				
Data set	LF-WtBE1	WtBE1-G6	LF-W610N	W610N-G7
X-ray source	KEK PF BL-5A	KEK PF AR NW12A	KEK PF AR NE3A	KEK PF AR NW12A
Detector	ADSC Quantum 315r	ADSC Quantum 270	PILATUS 2 M	ADSC Quantum 270
Wavelength (Å)	1.00000	1.00000	1.00000	1.00000
Space group	$P4_12_12$	$P4_12_12$	$P4_12_12$	$P4_12_12$
Unit-cell parameters (Å)	$a = 133.75$, $b = 133.75$, $c = 185.90$	$a = 134.13$, $b = 134.13$, $c = 184.32$	$a = 133.62$, $b = 133.62$, $c = 185.25$	$a = 134.03$, $b = 134.03$, $c = 185.06$
Resolution range (Å)	50.00 to 1.85 (1.88 to 1.85)	50.00 to 3.00 (3.05 to 3.00)	50.00 to 1.80 (1.83 to 1.80)	50.00 to 2.30 (2.34 to 2.30)
R_{merge}	0.074 (0.274)	0.128 (0.322)	0.041 (0.198)	0.075 (0.261)
Completeness (%)	100.0 (100.0)	99.8 (100.0)	100.0 (100.0)	100.0 (100.0)
Multiplicity	14.6 (14.8)	13.9 (14.4)	13.2 (13.1)	14.5 (14.6)
Average I/σ (I)	61.0 (10.7)	40.17 (15.12)	44.8 (9.0)	52.5 (15.1)
Unique reflections	143,511 (7126)	34,353 (1679)	154,705 (7650)	75,270 (3702)
Total reflections	2,096,822	476,549	2,036,638	1,088,438
Refinement statistics				
Resolution	47.29 to 1.85 (1.90 to 1.85)	47.42 to 3.00 (3.08 to 3.00)	47.24 to 1.80 (1.85 to 1.80)	47.38 to 2.30 (2.36 to 2.30)
R-factor	0.148 (0.163)	0.166 (0.211)	0.150 (0.164)	0.151 (0.156)
R_{free}-factor	0.170 (0.200)	0.224 (0.340)	0.171 (0.205)	0.184 (0.227)
RMSD from ideal value				
Bond lengths (Å)	0.028	0.014	0.026	0.021
Bond angles (degrees)	2.340	1.890	2.230	2.194
No. of water molecules	852	166	863	530
Average B-value	25.5	40.7	22.1	26.8
Ramachandran plot				
Favored region (%)	97.9	95.6	98.3	97.6
Allowed region (%)	1.9	4.2	1.6	2.1
Outlier region (%)	0.3	0.1	0.1	0.3

GH13_9 subfamily isoforms (2, 16). The three GH13_9 BE isoforms from ATCC 51142 and NBRC 102756 have been characterized, and it was found that BE1 and BE2 transferred short glucan chains with a degree of polymerization (DP) of 6–7, whereas BE3 transferred short as well as long glucan chains (DP 30) (17, 18).

Structural determination of the protein is an important factor for studying the catalytic mechanism of enzymes. Three-dimensional structures of BEs from *Escherichia coli* (EcBE) (19), *Mycobacterium tuberculosis* H37RV (MtBE) (20), *Oryza sativa* (OsBEI) (21), and *Homo sapiens* (HsBE) (22) have been solved to date. These studies provided basic information on the overall and domain structures of GH13_9 (prokaryotic)- and GH13_8 (eukaryotic)-type BEs. The structures of OsBEI (23), HsBE (22), and EcBE (24, 25) in complex with linear maltooligosaccharides or cyclodextrins led to the identification of surface binding sites (SBSs) located on the enzyme surface at certain distances from the active site (26–29). Possible roles of SBSs (substrate targeting, guiding substrate into the active site, and passing on reactions products) have been proposed (27). However, bound oligosaccharides have never been identified in the active site cleft of BE structures. The interactions of glucan chains at both the active site cleft and SBSs may provide important clues for understanding the reaction mechanism and mode of substrate binding of BEs.

In the present study, we determined the crystal structures of BE1 from ATCC 51142 (cceBE1), including ligand-free wild-type BE1 (ligand-free WtBE1 (LF-WtBE1)) and the W610N mutant (where Trp^{610} was replaced by Asn) in complex with G7 (W610N-G7). These structures revealed the unprecedented arrangement of the domains of cceBE1. Furthermore, the structure of W610N-G7 revealed for the first time the mode of oligosaccharide binding at the active site cleft. The significance of sugar binding at two SBSs was also identified. Based on the experimental evidence, we propose the substrate-binding model of cceBE1.

Results

Overall Structure of cceBE1—The crystal structure of LF-WtBE1 was determined at 1.85 Å resolution (Table 1). All of the protein crystals analyzed in this study (as described below) contained one molecule each per asymmetric unit. All BE1 structures, including LF-WtBE1, contained 755 residues (residues 5–759 of 1–773) with no disordered region (Fig. 1*A*). The cceBE1 comprised domain N (residues 5–99), CBM48 (residues 100–206), the catalytic domain known as domain A (residues 207–651), and domain C (residues 652–759) (Fig. 1, *A* and *B*). Domain A had a $(\beta/\alpha)_8$-barrel fold common to all proteins belonging to GH13, whereas domain N, CBM48, and domain C adopted β-sandwich folds. The arrangement of domains in cceBE1 was unprecedented among the available BE structures in that domain N was located at the back (opposite to the active site cleft) of the protein (Fig. 1*C*). The relative position of the domains was stabilized by three hydrogen bonds and nine van der Waals contacts between domain N and CBM48 in addition to four hydrogen bonds and nine van der Waals contacts between domain N and domain A. Apart from this work, only one study has reported the crystal structure of BE (MtBE) determined with domain N (20). In MtBE (20), domain N was located at one end of the elongated protein, making contact only with CBM48 via 10 hydrogen bonds and 26 van der Waals contacts (Fig. 1*C*). Excluding domain N, the overall structure of cceBE1 was similar to those of previously reported BEs, including EcBE (PDB code 1M7X; root mean square deviation (RMSD) for 569

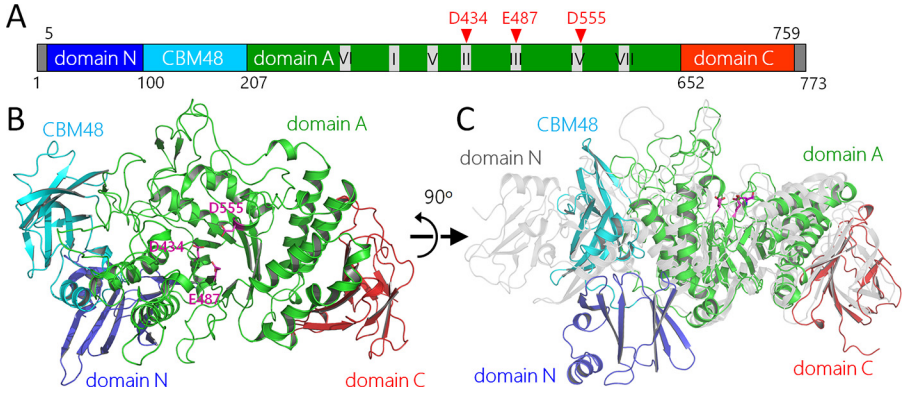

FIGURE 1. **Structure of WtBE1.** *A*, the domain structure of WtBE1. Domain N (residues 5–99), CBM48 (residues 100–206), domain A (catalytic domain, residues 207–651), and domain C (residues 652–759) in WtBE1 are indicated as *blue*, *cyan*, *green*, and *red boxes*, respectively. The structures of the N-terminal (residues 1–4) and C-terminal (residues 760–773) regions were not determined, and they are shown in *gray*. The seven consensus sequence regions (*I–VII*) in the GH13 α-amylase family are indicated by *gray boxes* (46). *Red arrowheads* denote the nucleophile (Asp^{434}), acid/base catalyst (Glu^{487}), and second conserved Asp (Asp^{555}). *B*, overall structure of LF-WtBE1 depicted in a *ribbon representation* and *colored* as described for *A*. The catalytically important residues Asp^{434}, Glu^{487}, and Asp^{555} are shown as *magenta sticks*. *C*, superimposed models of LF-WtBE1 and BE from *M. tuberculosis* H37RV (MtBE; PDB code 3K1D) (20). WtBE1 is *colored* as described for *A*, and MtBE is presented in *light gray*. The models are rotated by 90° along the *horizontal axis*.

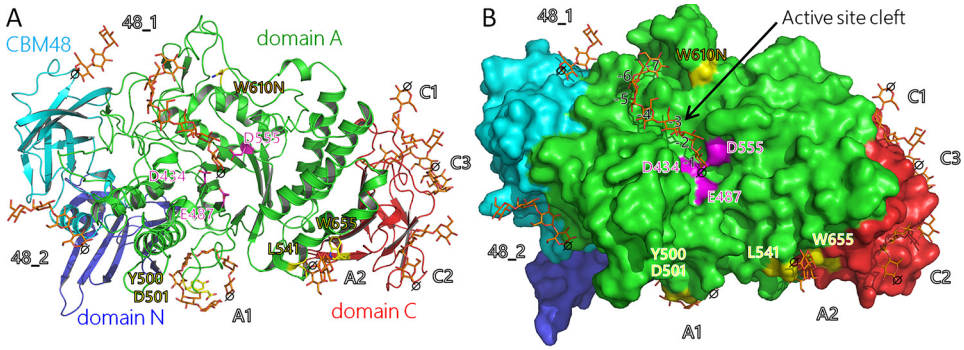

FIGURE 2. **Structure of the W610N mutant in complex with maltoheptaose.** *A*, *ribbon representation* of the overall structure of W610N-G7. Each domain in W610N-G7 is *colored* as described for Fig. 1*A*. The bound maltooligosaccharides are shown as *orange stick models*. Reducing ends of the sugars are marked with ϕ. The catalytically important residues (Asp^{434}, Glu^{487}, and Asp^{555}) and mutated residues (W610N) are shown as *magenta* and *yellow stick models*, respectively. Seven SBSs are *labeled*. Important residues for substrate binding (Tyr^{500}, Asp^{501}, Leu^{541}, and Trp^{655}) in A1 and A2 sites are *colored* in *yellow*. *B*, surface structure of W610N-G7. The active site cleft is indicated by an *arrow*. Subsites −7 to −1 are *labeled*.

Cα atoms is 1.08 Å) (19), MtBE (3K1D; RMSD for 596 Cα atoms is 0.98 Å) (20), OsBEI (3AML; RMSD for 550 Cα atoms is 1.75 Å) (21), and HsBE (4BZY; RMSD for 553 Cα atoms is 1.64 Å) (22). When only domain N was considered, its structure was highly similar between cceBE1 and MtBE (Z score = 10.5; RMSD for 99 Cα atoms = 2.5 Å), as revealed by a structural homology search using the DALI server (30).

Binding of Oligosaccharides at the Active Site—Site-directed mutational analyses were performed extensively in this study for amino acid residues around the active site and the known carbohydrate binding sites. The W610N mutant was created because Trp^{610} is positioned close to the active site, and it displays sequence variation between the related species (17). The mutant enzyme displayed alterations in catalytic specificity, which prompted us to determine its crystal structure as a ligand-free form or in complex with maltohexaose (G6) or maltoheptaose (G7).

The crystal structure of the W610N mutant in complex with G7 (W610N-G7) was determined at 2.3 Å resolution (Table 1). The oligosaccharide molecule was observed at the active site cleft (Fig. 2, *A* and *B*) for the first time in the crystal structure of BE. An electron density map of the bound sugar molecule in the active site cleft was shown in Fig. 3*A*. The amino acid residues, namely Pro^{217}, Glu^{284}, Trp^{285}, Phe^{323}, Asp^{324}, Trp^{327}, Tyr^{329}, Gln^{330}, Asp^{373}, Trp^{399}, His^{554}, and Asp^{555}, involved in recognition of the G7 molecule bound at subsites −7 to −1 are shown in Fig. 4*B*. Catalytically important residues in the α-amylase family, including the nucleophile (Asp^{434}), acid/base catalyst (Glu^{487}), and second aspartate (Asp^{555}), were located at subsite −1 (Figs. 1*A* and 5*A*). The hydrogen bonds and van der Waals contacts between the protein and G7 are summarized in Table 2. The G7 molecule adopted a twisted "S" conformation, as shown previously in the structure of barley α-amylase 1 (Amy1; another related enzyme belonging to GH13_6 subfamily) (Fig. 2, *A* and *B*) (31). A similar binding mode of G7 was also observed in debranching enzyme (isoamylase 1) from *Chlamydomonas reinhardtii* (CrISA1; belonging to GH13_11 subfamily) (32). The G7 molecule reported in CrISA1 was superimposed onto the W610N-G7 structure (Fig. 5*B*). The binding modes of the G7 molecules in both structures were apparently identical to each other except that in W610N-G7, the pyranose ring of Glc801 (at the reducing end, as shown in Fig. 5*B*) was rotated by 91° so that the O1 atom of Glc801 obstructed the position of the Oδ1 atom of the catalytic Asp^{434}. By contrast, G7 in CrISA1 was covalently attached to the catalytic Asp^{452} (CrISA1 numbering) to form a glycosylated intermediate (32).

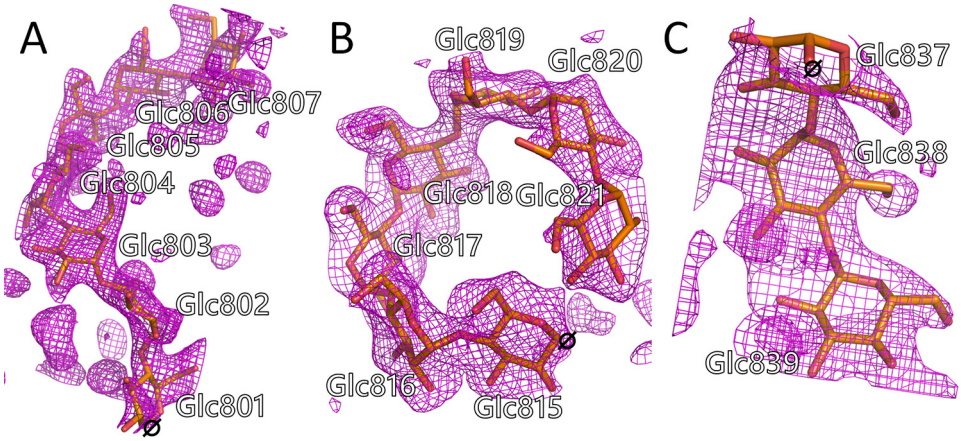

FIGURE 3. **$F_o - F_c$ omit electron density maps of the bound maltooligosaccharides in the W610N mutant in complex with maltoheptaose calculated from the final refined structure.** All maps were contoured at 2.0σ. *A*, map of the maltoheptaose unit bound at the active site cleft. *B*, map of the maltoheptaose unit bound at the A1 site. *C*, map of the maltotriose unit bound at the A2 site. The glucose units are shown as *orange stick models* and *numbered* according to coordinate files.

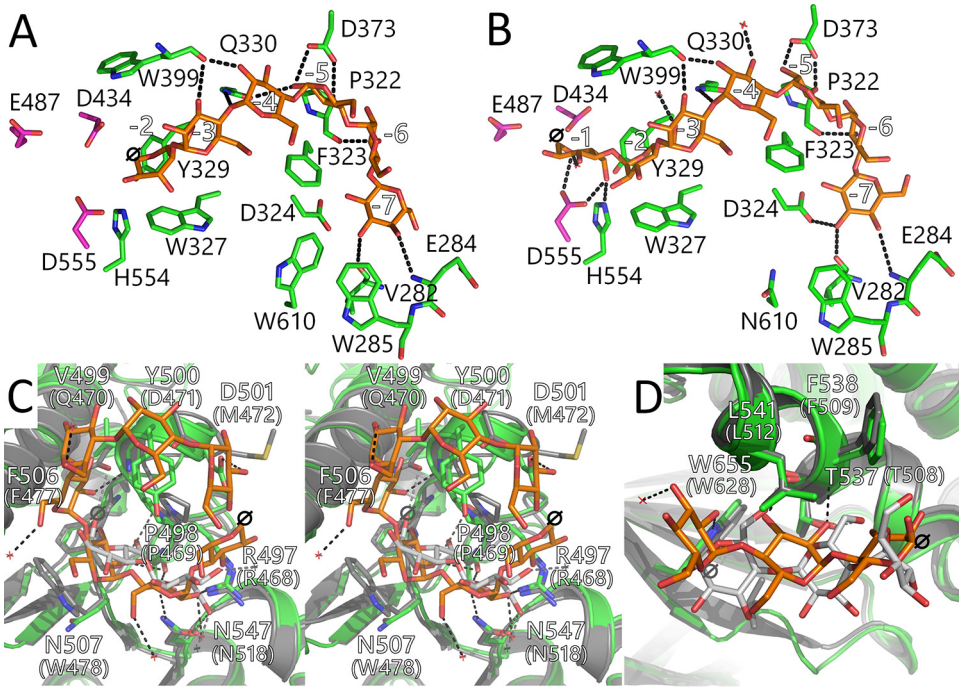

FIGURE 4. **Sugar-binding structures of WtBE1 and the W610N mutant in the active site cleft, A1 site, and A2 site.** *A*, G6 molecule bound to the active site cleft of WtBE1-G6. Residues participating in recognition of the G6 molecule are shown as *green stick models*. Catalytically important residues are indicated as *magenta sticks*. The bound G6 molecule is shown as an *orange stick model*. Reducing ends of the sugars are marked with ϕ. Subsites are *labeled* from -7 to -2. The estimated hydrogen bonds are shown as *dashed lines*. *B*, maltoheptaose (G7) molecule bound to the active site cleft of W610N-G7. *Stick models* are *colored* as described for *A*. The subsites are *labeled* from -7 to -1. *C*, stereo view of the superimposed structures of the A1 site in W610N-G7 and binding site III in EcBE in complex with G7 (PDB code 4LPC) (24). W610N-G7 and EcBE are *colored* in *green* and *gray*, respectively. Residues involved in recognition of the bound sugars are indicated by *stick models*. Residue numbers within and without *parentheses* indicate W610N-G7 and EcBE numbering, respectively. Sugars bound to W610N-G7 and EcBE are shown as *orange* and *white sticks*, respectively. Reducing ends of the sugars in W610N-G7 and EcBE are marked with *black* and *gray* ϕ, respectively. *D*, superimposed structure of the A2 site of W610N-G7 and binding site VI of EcBE. Sugar molecules are indicated as described for *C*.

In W610N-G7, the Oδ1 and Oδ2 atoms of Asp^{555} and the Nϵ2 atom of His^{554} hydrogen bonded to the O6, O5, and O6 atoms of Glc801, respectively (Table 2). The consecutive Asp and His residues are highly conserved in GH13 enzymes, and they typically form hydrogen bonds with the O2 and O3 atoms of the Glc unit at subsite -1 (33). The orientation of Glc801 was therefore unusual, and it may not represent the physiological state of the Glc residue, because it was not covalently bound to the protein (Figs. 4*B* and 5*B* and Table 2).

In addition to W610N-G7, the crystal structures of WtBE1 in complex with G6 (WtBE1-G6) and the ligand-free from of W610N (LF-W610N) were determined at 3.0 and 1.8 Å resolution, respectively (Table 1). The RMSD values between any combinations of the crystals shown in Table 1 were 0.22 Å or smaller (for 755 Cα atoms), indicating that cceBE1 did not undergo significant structural changes upon the W610N mutation or binding of maltooligosaccharides. In the WtBE1-G6 structure, a G6 molecule was found in subsites -7 to -2 of the

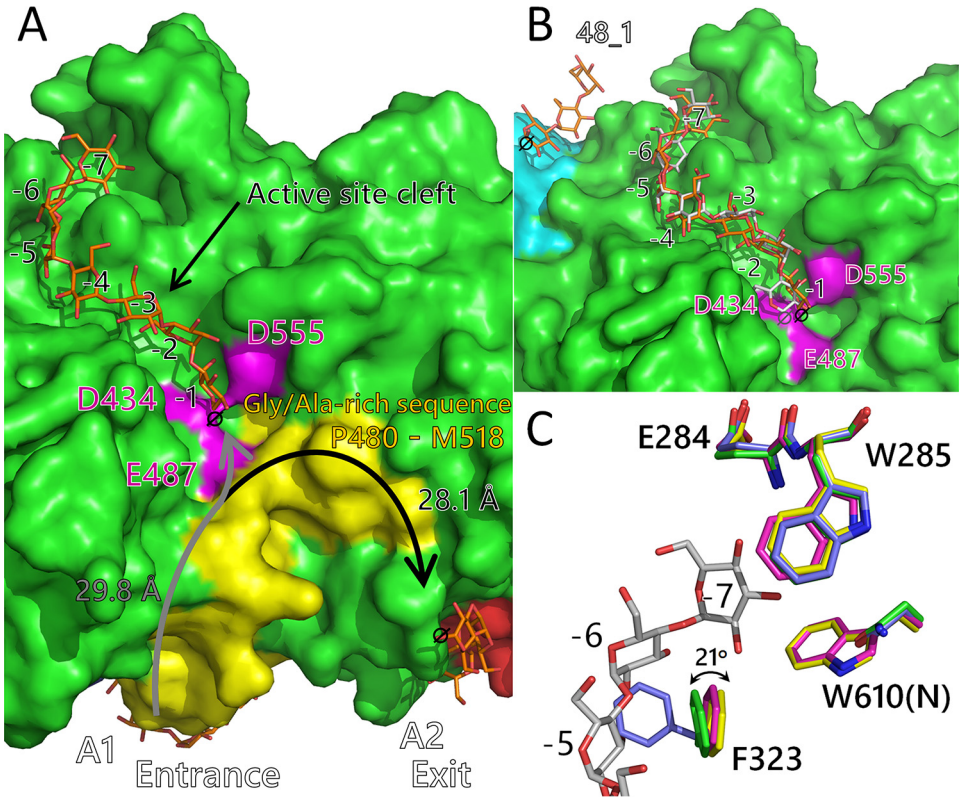

FIGURE 5. **Structures of the active site cleft in W610N-G7.** *A, surface representation* around the active site cleft, A1 site (entrance), and A2 site (exit) of W610N-G7. The catalytically important residues (Asp^{434}, Glu^{487}, and Asp^{555}) are indicated by *magenta*. The bound sugars at subsites (−7 to −1) are shown as *orange stick models*. The subsites, A1 site, and A2 site are *labeled*. The Gly/Ala-rich sequence connecting the A1 and A2 sites (Pro^{480}–Met^{518}) is indicated by *yellow*. The assumed path of the glucan chain between the A1 site and catalytic residue Asp^{434} is indicated by a *gray arrow*, and the distance is shown. The path between the catalytic residue and A2 site is indicated by a *black arrow*, and the distance is shown. *B*, superimposed structure of bound sugars in W610N-G7 and isoamylase 1 from *C. reinhardtii* (CrISA1) in complex with G7 (PDB code 4OKD) (32). The G7 molecule bound to the active site cleft of CrISA1 is superimposed on the surface model of W610N-G7. Domains in W610N-G7 are *colored* as described for Fig. 2*B*. The catalytically important residues (Asp^{434}, Glu^{487}, and Asp^{555}) are *colored* in *magenta*. The bound sugars in W610N-G7 and CrISA1 are shown as *orange* and *white stick models*, respectively. *Black* and *gray* ϕ indicate the reducing end of the bound sugars in W610N-G7 and CrISA1, respectively. The sugar-binding site (48_1) and subsites (−7 to −1) are *labeled*. *C*, superimposed structure of LF-WtBE1, WtBE1-G6, LF-W610N, and W610N-G7. Residues around subsites −7 to −5 of LF-WtBE1, WtBE1-G6, LF-W610N, and W610N-G7 are shown as *yellow*, *magenta*, *blue*, and *green stick models*, respectively, and *labeled*. Change in the χ^2 angle of Phe^{323} is *labeled*. The bound sugar in W610N-G7 is shown as a *white stick model*.

active site cleft (Fig. 4*A*), although the average *B*-factor for the G6 molecule was high (106.7 Å^2). The amino acid residues involved in the formation of subsites −7 to −2 were essentially the same as those in the W610N-G7 structure (Fig. 4*B*) except that the indole ring of Trp^{610} was eliminated in W610N and subsite −1 was empty in WtBE1-G6. The crystal structure of WtBE1 in complex with G7 (WtBE1-G7) was also determined at 2.0 Å resolution (data not shown). In contrast to WtBE1-G6 or W610N-G7, the G7 molecule was not observed in the active site cleft of the WtBE1-G7 structure, suggesting lower affinity of the active site cleft for G7 in WtBE1 than in W610N.

Conformation of the residues forming the subsites (−7 to −1) was unchanged in all crystal structures excluding Phe^{323}. In WtBE1, the orientation of the side chains of Phe^{323} was identical in LF-WtBE1 and WtBE1-G6 (Fig. 5*C*). In LF-W610N, however, the side chain of Phe^{323} moved largely to the active site cleft so that it obstructed the binding of the oligosaccharide at subsite −5 (Fig. 5*C*). By contrast, the Phe^{323} side chain in W610N-G7 was in a position close to that in WtBE1 so that the G7 molecule could be accommodated in the active site cleft. The average *B*-factor for the side chain of Phe^{323} in LF-W610N was 36.1 Å^2 (the average *B*-factor of the entire protein was 21.3 Å^2), as compared with 33.5 Å^2 (23.9 Å^2) in LF-WtBE1. The increase of the values for the side chain of Phe^{323} is attributed to elimination of the interaction between the side chains of Trp^{610} and Phe^{323}. In WtBE1, the aromatic ring of Phe^{323} was stabilized only by the CH/π interaction with the indole ring of Trp^{610} at a distance of 3.7 Å (Fig. 5*C*). The CH/π interaction was abolished by mutation of Trp^{610}, resulting in the altered conformation of Phe^{323} in W610N. Although the side chain of Phe^{323} in W610N-G7 was close to that in WtBE1, the χ^2 angle was rotated by 21° relative to that in WtBE1 structures (Fig. 5*C*). Consequently, the aromatic ring of Phe^{323} formed a stacking interaction with Glc805 at subsite −5 in W610N-G7 (Figs. 4*B* and 5*C* and Table 2). The average *B*-factor for Glc unit at subsite −5 was 40.5 Å^2 (among a range of 40.5–56.4 Å^2 for individual Glc units of G7) in W610N-G7 and 106.2 Å^2 (96.2–126.1 Å^2 for Glc units of G6) in WtBE1-G6. The much smaller value in W610N-G7 indicates that the Glc residue was stabilized more rigidly at subsite −5 than that in WtBE1. Furthermore, the W610N mutation resulted in the expansion of subsite −7, probably facilitating the binding of G7.

TABLE 2
Interactions between bound sugars and amino acid residues in W610N-G7

Glc unit		Residue	Distance (Å)
Active site cleft		*(donor substrate binding site)*	
Glc801**	O5	Asp434 Od1	2.4
	O5	Asp555 Od2	3.1
	O5	Wat1155**	2.8
	O6	His554 Ne2	2.8
	O6	Asp555 Od1	2.6
		Tyr329	VDW*
Glc802**	O6	Wat1158**	2.8
		Trp327	VDW*
Glc803**	O3	Trp399 O	2.7
	O4	Gln330 Ne2	3.1
		Phe323	VDW*
		Gly325	VDW*
Glc804**	O2	Trp399 O	2.7
	O3	Wat978**	2.7
		Phe323	VDW*
Glc805**	O2	Asp373 Od1	2.5
	O3	Asp373 Od2	2.5
		Phe323	VDW*
Glc806**	O2	Wat1008**	3.4
	O3	Pro322 O	2.8
		Pro217	VDW*
		Phe323	VDW*
Glc807**	O3	Val282 O	3.1
	O3	Asp324 Od2	2.9
	O4	Glu284 N	3.5
		Arg216	VDW*
A1			
Glc815**		-	
Glc816**	O2	Arg497 Nh1	3.4
	O2	Wat1167**	2.8
	O3	Ser496 O	3.3
	O3	Asn547 Nd2	3.0
	O6	Wat1161**	2.9
		Leu247	VDW*
Glc817**	O2	Ser496 O	3.4
	O2	Phe506 O	2.7
	O3	Gly505 O	2.6
		Pro498	VDW*
Glc818**	O2	Val499 N	2.9
	O6	Wat984**	2.7
		Tyr500	VDW*
Glc819**	O6	Wat1005**	2.6
		Tyr500	VDW*
Glc820**		Tyr500	VDW*
Glc821**	O3	Asp501 Od1	3.0
		Tyr500	VDW*
A2			
Glc837**		Phe538	VDW*
		Leu541	VDW*
Glc838**	O2	Thr537 Og1	2.6
	O2	Phe538 N	3.3
	O3	Thr537 O	2.7
		Leu541	VDW*
Glc839**	O2	Trp655 Ne1	2.8
	O3	Met540 O	2.7
	O3	Wat1106**	2.8
		Leu541	VDW*

* van der Waals contacts between carbon atoms in Glc units and those in residues (within 4.4 Å).
** The glucose units and water molecules are numbered according to coordinate files.

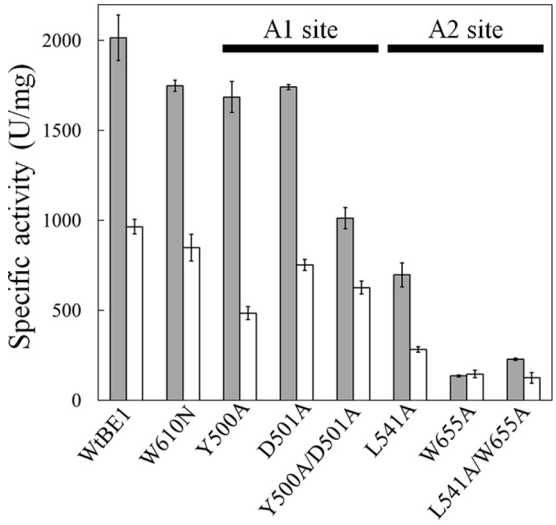

FIGURE 6. **Specific activity of WtBE1 and its mutants.** The specific activity of the enzymes was determined using 1 mg/ml amylose (*gray bars*) and 5 mg/ml amylopectin from potato (*white bars*) as substrates. Detailed reaction conditions were described previously (17, 18). Data are presented as the means ± S.D. (*error bars*) from three replicate experiments with independently prepared materials.

The mutant protein W610N retained the enzymatic activity, which reached ~90% of that in WtBE1 with amylose and amylopectin (Fig. 6). The relative abundance of each length of glucan chains was analyzed after enzymatic cleavage of α-1,6-linkages in the reaction products. Significant alteration ($p < 0.05$) was observed in the proportions of G6 and G7 between WtBE1 and W610N. The proportion of G6 in the reaction product of W610N was decreased from 31.9 to 17.9%, whereas that of G7 increased from 14.6 to 21.2% (Fig. 7, *A* and *B*).

Sugar-binding Mode and Mutational Analysis of Two SBSs (A1 and A2 Sites)—In addition to the active site cleft, oligosaccharides were bound at seven sites on the surface of the protein in the WtBE1-G6 and W610N-G7 structures (Fig. 2). These binding sites, considered to be SBSs, were designated as 48_1 and 48_2 (in CBM48), A1 and A2 (in domain A), and C1, C2, and C3 (in domain C) (Fig. 2, *A* and *B*). Among them, the C2 and C3 sites have not been described previously in any BE structure. In EcBE (PDB code 4LPC), oligosaccharide binding was found at SBSs corresponding to the 48_1, A1, A2, and C1 sites (24). In OsBEI (PDB code 3VU2), sugar chains were bound at SBSs corresponding to the 48_1 and 48_2 sites (23). The binding of sugars to an SBS equivalent to the 48_2 site was also observed in HsBE (PDB code 5CLW) (22). The electron densities for sugar molecules bound to W610N-G7 were of good quality, and sugar molecules were unambiguously modeled into the structure. The electron density maps of the bound sugar molecules in the A1 and A2 sites are shown in Fig. 3, *B* and *C*, respectively. The average *B*-factor for all bound oligosaccharide molecules in W610N-G7 was 47.7 Å^2, which was the smallest among all known BE structures, including EcBE in complex with G7 (PDB code 4LPC; 83.7 Å^2) (24) or β-cyclodextrin (5E6Z; 58.4 Å^2) (25), OsBEI in complex with G5 (3VU2; 62.7 Å^2) (23), and HsBE in complex with G7 (5CLW; 72.0 Å^2) (22).

Among the seven SBSs on the surface of W610N-G7, two SBSs (A1 and A2 sites) in domain A were located close to the active site and were therefore subjected to detailed analysis. In the A1 site, the G7 molecule was found in a helical conformation, wrapping around the side chains of Pro^{498} and Tyr^{500} (Fig. 4*C*). The hydroxyl groups of the G7 molecule were recognized by Leu^{247}, Ser^{496}, Arg^{497}, Val^{499}, Asp^{501}, Gly^{505}, Phe^{506}, and Asn^{547} through eight direct hydrogen bonds and four water-mediated hydrogen bonds (Fig. 4*C* and Table 2). van der Waals contacts were also involved in the binding of the sugar (Table 2). The A1 site corresponds to sugar-binding site III described in EcBE (24), in which the maltose (G2) portion of G7 was bound. However, the important Tyr^{500} and Asp^{501} residues in cceBE1 were replaced by Asp^{471} and Met^{472}, respectively, in EcBE. The positions of the bound sugars overlapped, although the orientation of the sugar chains was opposite to each other in the two structures (Fig. 4*C*).

Amino acid residues Tyr^{500} and Asp^{501} in A1 site were substituted by Ala to construct Y500A, D501A, and Y500A/D501A mutants. The activity of Y500A and D501A was reduced by only 10%, whereas that of the Y500A/D501A double mutant was decreased by 50% (Fig. 6). The chain length profile of the reaction product did not change compared with that of WtBE1 (not shown).

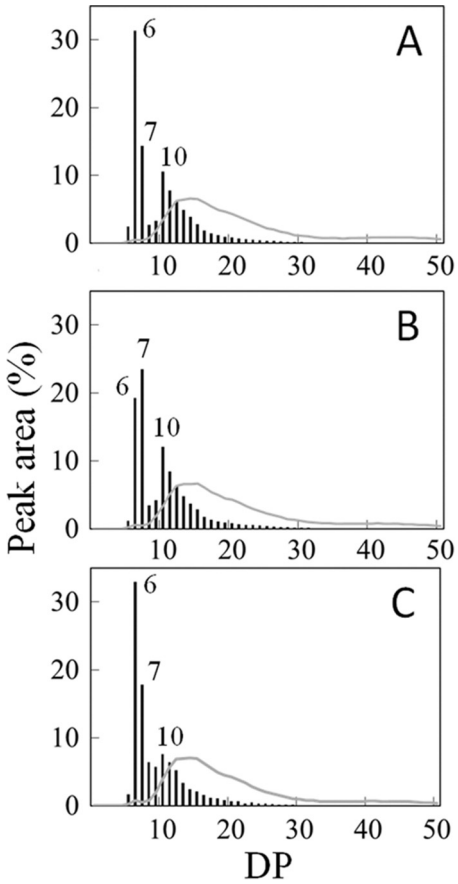

FIGURE 7. **Chain length distributions of debranched enzymatic reaction products using *ae*-amylopectin as a substrate.** *A*, chain length distributions of products formed by reaction with WtBE1. The data were excerpted from Hayashi *et al.* (18). *B*, chain length distributions of products formed by reaction with the W610N mutant. *C*, chain length distributions of products formed by reaction with L541A. *Black bars*, chain length distributions of the reaction products of each enzyme. *Gray lines*, chain length distributions of *ae*-amylopectin. The *x* and *y* axes denote the degree of polymerization of each chain and molar percentage of each chain, respectively. Representative data are shown from three replicate experiments with independently prepared materials. S.D. values for each molar percentage between the experiments were 1.2% or smaller.

The A2 site had the maltotriose (G3) portion of the G7 molecule in a slightly curved conformation around Leu^{541} (Fig. 4*D*). Thr^{537}, Phe^{538}, Met^{540}, Trp^{655}, and a water molecule (Wat^{1106}) formed hydrogen bonds with the hydroxyl groups of the bound G3 unit, and Phe^{538} and Leu^{541} had van der Waals interactions with the sugar molecule (Fig. 4*D* and Table 2). Sugar-binding site VI described in EcBE (24), corresponding to the A2 site, had the G3 portion of G7, and important amino acids for recognition of the maltooligosaccharide were conserved (Fig. 4*D*). The bound sugars overlapped each other with some minor deviations, but they were oriented in the opposite directions (Fig. 4*D*).

Enzymatic activities were markedly reduced in the L541A, W655A, and L541A/W655A mutants (Fig. 6). Furthermore, the relative abundance of maltodecaose (G10) was significantly reduced ($p < 0.05$) in L541A (7.9%) compared with that in WtBE1 (10.6%) (Fig. 7*C*). Conversely, the relative proportions of G7, maltooctaose (G8), and maltononaose (G9) were increased in L541A (17.5, 6.2, and 5.6%, respectively) compared with those in WtBE1 (14.6, 2.6, and 3.1%, respectively). The results suggest that mutation of Leu^{541} substantially impaired binding at the A2 site of glucan chains, especially G10, possibly serving as a substrate (see "Discussion"). In addition, a preliminary structural analysis indicated that the W655A mutation resulted in the local disruption of an α-helix facing the indole ring of Trp^{655}, leading to the profound reduction of the enzymatic activity accompanied by altered (amylose/amylopectin) specificity.

Discussion

To obtain structural insight into the reaction mechanism of BE, we have attempted to crystallize various BEs (in recombinant forms) from several cyanobacterial species, including *Synechococcus elongatus* PCC 7942 and *Cyanobacterium* sp. NBRC 102756 (17). Although most of the proteins were poorly crystallized, cceBE1 was found to yield crystals (18) suitable for structural analysis, as reported in this study. Of the four domains in cceBE1, the position of domain N was highly distinct from that of previously reported MtBE (Fig. 1*C*), whereas the structures of individual domains were similar between these proteins. The difference arose from the arrangement of a loop between domain N and CBM48 (Fig. 1*C*). The three-dimensional arrangement of the domains was not predicted by the primary structure, and it is possible that the relative location of domain N in other BEs from some bacteria (especially from cyanobacteria) is similar to that of cceBE1.

Previous studies of EcBE and BE from *Vibrio vulnificus* illustrated that domain N is involved in the determination of enzyme specificity by influencing the lengths of the produced glucan chains (34, 35). Replacement of WtBE in a cyanobacterium *Synechocystis* sp. PCC 6803 with N-terminally truncated forms resulted in the production of glycogen with altered lengths of glucan chains (36). This observation suggests that domain N of BE is involved in the determination of polysaccharide structure *in vivo*, presumably through interactions with other enzymes responsible for glucan metabolism. Whereas deletion of domain N in cceBE1 resulted in reduced stability of the protein during incubation at high temperatures, it did not affect the catalytic specificity toward *ae*-amylopectin, potato amylopectin, and potato amylose (not shown). It is possible, however, that these substrates did not fully represent the physiological state of the intermediary amylopectin structures during biosynthesis. No sugar-binding site was identified in domain N of cceBE1. Together with its position in the enzyme structure, there might be variation concerning the involvement of domain N in the modulation of catalytic specificity.

Crystal structures have been solved for BEs from both glycogen-producing (humans, *E. coli*, and *M. tuberculosis*) and starch-producing (rice and *Cyanothece*) organisms (19–22). However, no clear correlation has been found between the structure of individual BEs and the molecular properties of the α-glucans produced (glycogen or amylopectin) in the source organisms. Rather, amylopectin is synthesized in the presence of multiple BE isoforms with distinct properties (1, 7, 9, 38), as opposed to glycogen produced by the single BE isoform (2, 8, 10).

Binding of oligosaccharides in the active site cleft of BE was observed for the first time in the present study. In previous

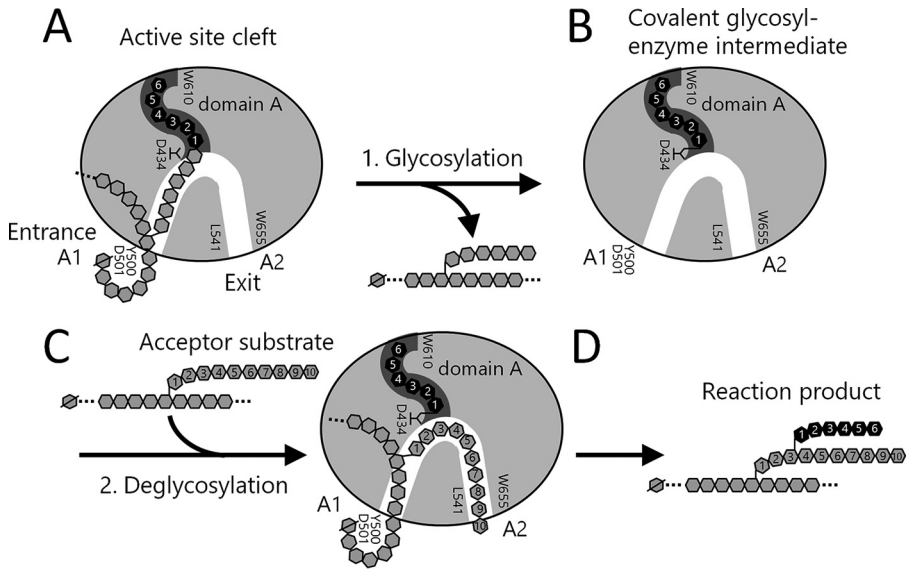

FIGURE 8. **Schematic drawing of the donor/acceptor substrate binding model of cceBE1.** *A*, donor substrate binding from the A1 site (entrance) to the active site cleft (subsites −7 to −1) via the Gly/Ala-rich sequence. The active site cleft is *colored dark gray*. The Gly/Ala-rich sequence is *colored white*. Glc units are indicated by hexagons. The Glc unit at the reducing end is indicated by a *slash mark*. Glc units to be transferred by BE1 are shown as *black hexagons* and *labeled* from subsite −1. *B*, covalent glycosyl-enzyme intermediate. Glc1 in subsite −1 is covalently bound to the nucleophile (Asp^{434}). *C*, acceptor substrate binding from the A1 site (entrance) to the A2 site (exit) via the Gly/Ala-rich sequence. Glc units in the acceptor substrate are *labeled* from the branch point. *D*, formation and liberation of the reaction product. A new branch point is frequently formed at third Glc unit from the existing branch point of the acceptor substrate. Detailed explanations of each step are described under "Discussion."

studies, sugar chains were found only at certain distances from the active site in the crystal structures (OsBEI (23), HsBE (22), and EcBE (24, 25)). Binding of the glucan chain at the active site was accomplished by soaking the protein crystals of cceBE1 in high concentrations of oligosaccharides, namely 500 mM G6 and 300 mM G7. The active site cleft of cceBE1 may have poor affinity for short oligosaccharides, such as G6 and G7, and the binding of longer glucans with DP ≥ 12 is required for the reaction to occur (24, 37–39). In WtBE1, G6 molecule was bound at subsites −7 to −2 (Fig. 4*A*) rather than −6 to −1. This mode of binding occurred probably because of the clash between the sugar chain and Asp^{434} at subsite −1, because the sugar chain was not covalently bound to the protein. It is also possible that the observed binding mode was due to higher affinities of subsites −7 through −2 than those of subsites −6 through −1. The binding of G6 (coordinate Glc801–Glc806) occurred despite the restriction of space at subsite −7 due to the presence of the indole ring (Cζ2 atom) of Trp^{610} positioned near the O3 atom of Glc806 (distance of 3.2 Å). In contrast to G6, binding of G7 was not observed (not shown), presumably because of the structural constraints both at subsites −7 and −1. When Trp^{610} was replaced by Asn in the W610N mutant, the binding of G7 was observed due to the widening of subsite −7 and stabilization by an interaction with Phe^{323} (Fig. 5*C*). Trp^{610} has therefore been identified as an important determinant of enzymatic specificity in cceBE1.

Among the seven SBSs identified in this study (Fig. 2, *A* and *B*), mutations at the A1 or A2 site affected the activity or specificity of the enzyme (Figs. 6 and 7), supporting the assumption that these sites are involved in substrate binding. The position and orientation of the sugar chains bound at A1 and A2 sites represent the binding mode, consistent with the idea that these sugar chains are portions of much longer glucans, one extending from A1 to the active site cleft and the other from A1 to A2 via the active site. We assume these glucan chains correspond to the donor and acceptor glucan chains, respectively, involved in the BE reaction.

It has been proposed that Gly/Ala-rich sequences, which are conserved in BEs (residues 480–518; cceBE1 numbering), serve as the binding surfaces for donor/acceptor glucan chains (22). The Gly/Ala-rich sequence lies near the active site connecting the A1 site, active site cleft, and A2 site in a bifurcating manner (Fig. 5*A*, *yellow*). Based on the orientation of the oligosaccharides found in the cceBE1 crystals, A1 and A2 sites are responsible for the binding of the reducing and non-reducing ends of glucan chains, respectively. The A1 and A2 sites are thus designated as the entrance and exit of glucan chains, respectively (Fig. 5*A*, *gray arrow*). The distance between the A1 site (non-reducing end of the bound G7) and the active site (Asp^{434}) was 29.8 Å, which can accommodate 7 Glc units. Assuming 7 Glc units in the A1 site, another 7 Glc units between the A1 and active sites, and 6 Glc units in the active site cleft, it is suggested that cceBE1 can bind glucan chains with 20 Glc units as a donor substrate. Because of the wide cleft, cceBE1 may bind glucan chains containing α-1,6 linkages, and thus, the length of α-1,4-linked (linear) glucan moiety at the non-reducing portion has a peak at DP 12. Cleavage of the sugar chain in the middle would produce G6, the major oligosaccharide species produced by cceBE1 (Fig. 7*A*). When Leu^{541} in the A2 site was substituted by Ala, the proportion of glucan chains with DP 10 (G10) was reduced (Fig. 7*C*). Leu^{541} is therefore responsible for preferential binding at the A2 site of G10, which may correspond to the acceptor glucan chain.

We propose a reaction model as shown in Fig. 8 to explain the mechanism by which A1, A2, and the active site cleft are engaged in the glycosylation and deglycosylation steps (Fig. 8). Binding of a long glucan chain (DP ≥ 12) may be stabilized by

interactions at multiple sites to form the enzyme-substrate complex, leading to the first step of the catalysis (glycosylation) (Fig. 8, *step A*). In the glycosylation step, the α-1,4-glucosidic linkage of the donor glucan chain is cleaved, and the glucan chain, preferentially G6 or G7, is covalently bound to the catalytic residue (nucleophile Asp^{434}) to form the glycosyl-enzyme intermediate (Fig. 8, *step B*), followed by release of the rest of the polysaccharide molecule from the enzyme. The second glucan chain extending from the A1 site via the Gly/Ala-rich sequence then binds to the enzyme with its non-reducing end attached to the A2 site (Figs. 5*A* (*black arrow*) and 8 (*step C*)). A previous study illustrated that, concerning the specificity of the acceptor chain, BEs from bacteria preferred to transfer the glucan chain to the previously unbranched chain, or "outer chain," in polysaccharide molecules (40). Moreover, bacterial BEs predominantly (if not exclusively) transferred glucan chains to the third Glc unit from the reducing end of the acceptor chain (40) (Fig. 8, *step C*). Glc1 of the donor glucan chain attached at Asp^{434} is subject to nucleophilic attack by the O6 atom of the Glc unit in the acceptor chain and consequently forms a new α-1,6-bond. Finally, the reaction product is released from the enzyme surface to complete the reaction (Fig. 8, *step D*).

The mode of substrate binding in the active site cleft of cceBE1 was similar to those of other GH13 enzymes. By contrast, there were differences in the orientation of oligosaccharide binding in SBSs between proteins (at both the A1 and A2 sites in cceBE1, corresponding to binding sites III and VI in EcBE, respectively). It is possible that the variation exists in the mode of oligosaccharide binding depending on the BE species, with opposite locations of the entrance and exit of glucan chains. Further structural analyses of other BEs with bound sugars are required to clarify whether variation exists in the mode of sugar binding in these sites among BEs. The remaining questions also include structural determinants that give rise to the catalytic specificity (preferred chain lengths transferred) in different BEs and the mechanism by which the water molecule is excluded in the deglycosylation reaction to prevent hydrolytic activity. Nevertheless, the structural evidence of cceBE1 reported in this study represents a crucial step for better understanding the reaction catalyzed by BEs and the engineering of BEs with altered specificity.

Experimental Procedures

Preparation of Purified Recombinant Enzymes, Enzyme Assay, and Chain Length Distribution Analyses of the Enzymatic Reaction Products—The expression plasmid pET15b-cceBE1 harboring *cce_2248* (2322 bp) was constructed previously (18). To facilitate purification using a Ni^{2+} affinity column, the N termini of all of the recombinant proteins used in this study were His_6-tagged. The expression plasmids of all mutants were constructed with a PrimeSTAR mutagenesis basal kit (TaKaRa Bio, Otsu, Japan) using pET15b-cceBE1 as the template. The following primer sets were used to construct the mutants: Y500A, 5′-TCCTGTTGCTGATGGTGGGTTAGGA-3′ (sense) and 5′-ACCATCAGCAACAGGACGAGACACT-3′ (antisense); D501A, 5′-GTTTATGCTGGTGGGTTAGGA-3′ (sense) and 5′-CCCACCAGCATAAACAGGACGAGACA-3′ (antisense); Y500A/D501A, 5′-GTTGCTGCTGGTGGGTTAGGA-3′ (sense) and 5′-CCCACCAGCAGCAACAGGACGAGACA-3′ (antisense); L541A, 5′-TAGTATGGCGTACTACTACAACGAAAACT-3′ (sense) and 5′-GTAGTACGCCATACTAAACGTGACGT-3′ (antisense); W655A, 5′-GTTTGAAGCGATCGATTGTAATGATA-3′ (sense) and 5′-ATCGATCGCTTCAAACCCATGATACT-3′ (antisense); L541A/W655A, 5′-GTTTGAAGCGATCGATTGTAATGATA-3′ (sense) and 5′-ATCGATCGCTTCAAACCCATGATACT-3′ (antisense); and W610N, 5′-TGAGTGGAATGTTAATGGGGACTTAGAATGGCAT-3′ (sense) and 5′-AGTCCCCATTAACATTCCACTCACTCCATTGACCA-3′ (antisense). Expression of the genes in *E. coli* BL21 (DE3) cells (Merck Millipore, Billerica, MA), purification of the recombinant proteins, determination of the enzymatic activities, and chain length distribution analyses of the reaction products were performed as described previously (17, 18).

Crystallography—WtBE1 and its mutant W610N were crystallized using the hanging drop vapor diffusion method, as described previously (18). In brief, 15 mg/ml protein solution (3 μl) was mixed with an equal volume of reservoir solution (0.1 M HEPES-NaOH (pH 7.2–7.9), 7–10% (w/v) ethanol, and 0.2 M $MgCl_2$) and equilibrated against 500 μl of reservoir solution at 20 °C. Crystals of WtBE1 and W610N suitable for X-ray analysis were obtained within a few weeks. Crystals of WtBE1 in complex with G6 (WtBE1-G6) were obtained by soaking crystals in reservoir solution containing 500 mM G6 for 30 min at room temperature. Crystals of W610N in complex with G7 (W610N-G7) were obtained by soaking crystals in reservoir solution containing 300 mM G7 for 30 min at room temperature. Diffraction data were collected using beamlines BL-5A (for LF-WtBE1 and WtBE1-G6), AR-NW12A (for LF-W610N), and AR-NE3A (for W610N-G7), at the Photon Factory, High Energy Accelerator Research Organization (Tsukuba, Japan) (λ = 1.00000 Å). Diffraction data were processed and scaled using the HKL2000 program (41).

The structure of LF-WtBE1 was determined by the molecular replacement method using the BALBES program (42). The structures of WtBE1-G6, LF-W610N, and W610N-G7 were determined by the same method using MOLREP (43), with the structure model of LF-WtBE1 serving as the template. Manual model rebuilding and refinement were performed using Coot (44) and REFMAC5 (45). The data collection and refinement statistics are shown in Table 1. The atomic coordinates and structure factors of LF-WtBE1, WtBE1-G6, LF-W610N, and W610N-G7 were deposited in the Protein Data Bank under the accession codes 5GQU, 5GQV, 5GQW, and 5GQX, respectively. The figures were drawn using PyMOL (Schrödinger, LLC, New York).

Author Contributions—M. H. and R. S. performed the experiments. M. H., R. S., N. F., and E. S. analyzed the results. C. C. and S. G. B. provided the materials. M. H., R. S., C. C., S. G. B., N. F., and E. S. designed the study. M. H., R. S., N. F., and E. S. wrote the paper.

Acknowledgments—We thank Drs. Sohei Ito, Takuya Ishida, Kiyohiko Igarashi, and Zui Fujimoto for help in conducting the study. We also thank the staff of the Photon Factory for the X-ray data collection. Pseudomonas isoamylase was generously provided by Hayashibara Co.

References

1. Tetlow, I. J., and Emes, M. J. (2014) A review of starch-branching enzymes and their role in amylopectin biosynthesis. *IUBMB Life* **66,** 546–558
2. Suzuki, E., and Suzuki, R. (2016) Distribution of glucan-branching enzymes among prokaryotes. *Cell Mol. Life Sci.* **73,** 2643–2660
3. Adeva-Andany, M. M., González-Lucán, M., Donapetry-García, C., Fernández-Fernández, C., and Ameneiros-Rodríguez, E. (2016) Glycogen metabolism in humans. *BBA Clin.* **5,** 85–100
4. Pfister, B., and Zeeman, S. C. (2016) Formation of starch in plant cells. *Cell Mol. Life Sci.* **73,** 2781–2807
5. Wilson, W. A., Roach, P. J., Montero, M., Baroja-Fernández, E., Muñoz, F. J., Eydallin, G., Viale, A. M., and Pozueta-Romero, J. (2010) Regulation of glycogen metabolism in yeast and bacteria. *FEMS Microbiol Rev.* **34,** 952–985
6. Suzuki, E., and Suzuki, R. (2013) Variation of storage polysaccharides in phototrophic microorganisms. *J. Appl. Glycosci.* **60,** 21–27
7. Nakamura, Y. (2002) Towards a better understanding of the metabolic system for amylopectin biosynthesis in plants: rice endosperm as a model tissue. *Plant Cell Physiol.* **43,** 718–725
8. Ball, S., Colleoni, C., Cenci, U., Raj, J. N., and Tirtiaux, C. (2011) The evolution of glycogen and starch metabolism in eukaryotes gives molecular clues to understand the establishment of plastid endosymbiosis. *J. Exp. Bot.* **62,** 1775–1801
9. Fujita, N. (2014) Starch biosynthesis in rice endosperm. *Agri-Biosci. Monogr.* **4,** 1–18
10. Deschamps, P., Colleoni, C., Nakamura, Y., Suzuki, E., Putaux, J. L., Buléon, A., Haebel, S., Ritte, G., Steup, M., Falcón, L. I., Moreira, D., Löffelhardt, W., Raj, J. N., Plancke, C., d'Hulst, C., *et al.* (2008) Metabolic symbiosis and the birth of the plant kingdom. *Mol. Biol. Evol.* **25,** 536–548
11. Cantarel, B. L., Coutinho, P. M., Rancurel, C., Bernard, T., Lombard, V., and Henrissat, B. (2009) The Carbohydrate-Active EnZymes database (CAZy): an expert resource for glycogenomics. Nucleic *Acids Res.* **37,** D233–D238
12. Stam, M. R., Danchin, E. G., Rancurel, C., Coutinho, P. M., and Henrissat, B. (2006) Dividing the large glycoside hydrolase family 13 into subfamilies: towards improved functional annotations of α-amylase-related proteins. *Protein Eng. Des. Sel.* **19,** 555–562
13. Murakami, T., Kanai, T., Takata, H., Kuriki, T., and Imanaka, T. (2006) A novel branching enzyme of the GH-57 family in the hyperthermophilic archaeon *Thermococcus kodakaraensis* KOD1. *J. Bacteriol.* **188,** 5915–5924
14. Reddy, K. J., Haskell, J. B., Sherman, D. M., and Sherman, L. A. (1993) Unicellular, aerobic nitrogen-fixing cyanobacteria of the genus *Cyanothece. J. Bacteriol.* **175,** 1284–1292
15. Nakamura, Y., Takahashi, J., Sakurai, A., Inaba, Y., Suzuki, E., Nihei, S., Fujiwara, S., Tsuzuki, M., Miyashita, H., Ikemoto, H., Kawachi, M., Sekiguchi, H., and Kurano, N. (2005) Some cyanobacteria synthesize semi-amylopectin type α-polyglucans instead of glycogen. *Plant Cell Physiol.* **46,** 539–545
16. Suzuki, E., Onoda, M., Colleoni, C., Ball, S., Fujita, N., and Nakamura, Y. (2013) Physicochemical variation of cyanobacterial starch, the insoluble α-glucans in cyanobacteria. *Plant Cell Physiol.* **54,** 465–473
17. Suzuki, R., Koide, K., Hayashi, M., Suzuki, T., Sawada, T., Ohdan, T., Takahashi, H., Nakamura, Y., Fujita, N., and Suzuki, E. (2015) Functional characterization of three (GH13) branching enzymes involved in cyanobacterial starch biosynthesis from *Cyanobacterium* sp. NBRC 102756. *Biochim. Biophys. Acta* **1854,** 476–484
18. Hayashi, M., Suzuki, R., Colleoni, C., Ball, S. G., Fujita, N., and Suzuki, E. (2015) Crystallization and crystallographic analysis of branching enzymes from *Cyanothece* sp. ATCC 51142. *Acta Crystallogr. F Struct. Biol. Commun.* **71,** 1109–1113
19. Abad, M. C., Binderup, K., Rios-Steiner, J., Arni, R. K., Preiss, J., and Geiger, J. H. (2002) The X-ray crystallographic structure of *Escherichia coli* branching enzyme. *J. Biol. Chem.* **277,** 42164–42170
20. Pal, K., Kumar, S., Sharma, S., Garg, S. K., Alam, M. S., Xu, H. E., Agrawal, P., and Swaminathan, K. (2010) Crystal structure of full-length *Mycobacterium tuberculosis* H37Rv glycogen branching enzyme: insights of N-terminal β-sandwich in substrate specificity and enzymatic activity. *J. Biol. Chem.* **285,** 20897–20903
21. Noguchi, J., Chaen, K., Vu, N. T., Akasaka, T., Shimada, H., Nakashima, T., Nishi, A., Satoh, H., Omori, T., Kakuta, Y., and Kimura, M. (2011) Crystal structure of the branching enzyme I (BEI) from *Oryza sativa* L with implications for catalysis and substrate binding. *Glycobiology* **21,** 1108–1116
22. Froese, D. S., Michaeli, A., McCorvie, T. J., Krojer, T., Sasi, M., Melaev, E., Goldblum, A., Zatsepin, M., Lossos, A., Álvarez, R., Escribá, P. V., Minassian, B. A., von Delft, F., Kakhlon, O., and Yue, W. W. (2015) Structural basis of glycogen branching enzyme deficiency and pharmacologic rescue by rational peptide design. *Hum. Mol. Genet.* **24,** 5667–5676
23. Chaen, K., Noguchi, J., Omori, T., Kakuta, Y., and Kimura, M. (2012) Crystal structure of the rice branching enzyme I (BEI) in complex with maltopentaose. *Biochem. Biophys. Res. Commun.* **424,** 508–511
24. Feng, L., Fawaz, R., Hovde, S., Gilbert, L., Chiou, J., and Geiger, J. H. (2015) Crystal Structures of *Escherichia coli* branching enzyme bound to linear oligosaccharides. *Biochemistry* **54,** 6207–6218
25. Feng, L., Fawaz, R., Hovde, S., Sheng, F., Nosrati, M., and Geiger, J. H. (2016) Crystal structures of *Escherichia coli* branching enzyme in complex with cyclodextrins. *Acta Crystallogr. D Struct. Biol.* **72,** 641–647
26. Nielsen, M. M., Bozonnet, S., Seo, E. S., Mótyán, J. A., Andersen, J. M., Dilokpimol, A., Abou Hachem, M., Gyémánt, G., Naested, H., Kandra, L., Sigurskjold, B. W., and Svensson, B. (2009) Two secondary carbohydrate binding sites on the surface of barley α-amylase 1 have distinct functions and display synergy in hydrolysis of starch granules. *Biochemistry* **48,** 7686–7697
27. Cuyvers, S., Dornez, E., Delcour, J. A., and Courtin, C. M. (2012) Occurrence and functional significance of secondary carbohydrate binding sites in glycoside hydrolases. *Crit. Rev. Biotechnol.* **32,** 93–107
28. Cockburn, D., Nielsen, M. M., Christiansen, C., Andersen, J. M., Rannes, J. B., Blennow, A., and Svensson, B. (2015) Surface binding sites in amylase have distinct roles in recognition of starch structure motifs and degradation. *Int. J. Biol. Macromol.* **75,** 338–345
29. Wilkens, C., Cockburn, D., Andersen, S., Petersen, B. O., Ruzanski, C., Field, R. A., Hindsgaul, O., Nakai, H., McCleary, B., Smith, A. M., Hachem, M. A., and Svensson, B. (2015) Analysis of surface binding sites (SBS) within GH62, GH13, and GH77. *J. Appl. Glycosci.* **62,** 87–93
30. Holm, L., and Rosenström, P. (2010) Dali server: conservation mapping in 3D. *Nucleic Acids Res.* **38,** W545–W549
31. Robert, X., Haser, R., Mori, H., Svensson, B., and Aghajari, N. (2005) Oligosaccharide binding to barley α-amylase 1. *J. Biol. Chem.* **280,** 32968–32978
32. Sim, L., Beeren, S. R., Findinier, J., Dauvillée, D., Ball, S. G., Henriksen, A., and Palcic, M. M. (2014) Crystal structure of the *Chlamydomonas* starch debranching enzyme isoamylase ISA1 reveals insights into the mechanism of branch trimming and complex assembly. *J. Biol. Chem.* **289,** 22991–23003
33. Uitdehaag, J. C., Mosi, R., Kalk, K. H., van der Veen, B. A., Dijkhuizen, L., Withers, S. G., and Dijkstra, B. W. (1999) X-ray structures along the reaction pathway of cyclodextrin glycosyltransferase elucidate catalysis in the α-amylase family. *Nat. Struct. Biol.* **6,** 432–436
34. Devillers, C. H., Piper, M. E., Ballicora, M. A., and Preiss, J. (2003) Characterization of the branching patterns of glycogen branching enzyme truncated on the N-terminus. *Arch. Biochem. Biophys.* **418,** 34–38
35. Jo, H. J., Park, S., Jeong, H. G., Kim, J. W., and Park, J. T. (2015) *Vibrio vulnificus* glycogen branching enzyme preferentially transfers very short chains: N1 domain determines the chain length transferred. *FEBS Lett.* **589,** 1089–1094
36. Welkie, D. G., Lee, B.-H., and Sherman, L. A. (2015) Altering the structure of carbohydrate storage granules in the cyanobacterium *Synechocystis* sp. PCC 6803 through branching enzyme truncations. *J. Bacteriol.* **198,** 701–710
37. Guan, H., Li, P., Imparl-Radosevich, J., Preiss, J., and Keeling, P. (1997) Comparing the properties of *Escherichia coli* branching enzyme and maize branching enzyme. *Arch. Biochem. Biophys.* **342,** 92–98

38. Nakamura, Y., Utsumi, Y., Sawada, T., Aihara, S., Utsumi, C., Yoshida, M., and Kitamura, S. (2010) Characterization of the reactions of starch branching enzymes from rice endosperm. *Plant Cell Physiol.* **51,** 776–794
39. Li, C., and Gilbert, R. G. (2016) Progress in controlling starch structure by modifying starch-branching enzymes. *Planta* **243,** 13–22
40. Sawada, T., Nakamura, Y., Ohdan, T., Saitoh, A., Francisco, P. B., Jr, Suzuki, E., Fujita, N., Shimonaga, T., Fujiwara, S., Tsuzuki, M., Colleoni, C., and Ball, S. (2014) Diversity of reaction characteristics of glucan branching enzymes and the fine structure of α-glucan from various sources. *Arch. Biochem. Biophys.* **562,** 9–21
41. Otwinowski, Z., and Minor, W. (1997) Processing of X-ray diffraction data collected in oscillation mode. *Methods Enzymol.* **276,** 307–326
42. Long, F., Vagin, A. A., Young, P., and Murshudov, G. N. (2008) BALBES: a molecular-replacement pipeline. *Acta Crystallogr. D Biol. Crystallogr.* **64,** 125–132
43. Vagin, A., and Teplyakov, A. (2010) Molecular replacement with MOLREP. *Acta Crystallogr. D Biol. Crystallogr.* **66,** 22–25
44. Emsley, P., and Cowtan, K. (2004) Coot: model-building tools for molecular graphics. *Acta Crystallogr. D Biol. Crystallogr.* **60,** 2126–2132
45. Murshudov, G. N., Skubák, P., Lebedev, A. A., Pannu, N. S., Steiner, R. A., Nicholls, R. A., Winn, M. D., Long, F., and Vagin, A. A. (2011) REFMAC5 for the refinement of macromolecular crystal structures. *Acta Crystallogr. D Biol. Crystallogr.* **67,** 355–367
46. Janeček, Š. (2002) How many conserved sequence regions are there in the α-amylase family? *Biologia* **57,** 29–41